

**Evidence for a size-selective adsorption mechanism on oxide surfaces:
Pd and Au atoms on SiO₂/Mo(112)**

Stefan Ulrich, Niklas Nilius^{*}, Hans-Joachim Freund
*Fritz-Haber-Institut der MPG
Berlin, Germany*

Umberto Martinez, Livia Giordano, Gianfranco Pacchioni[#]
*Dipartimento di Scienza dei Materiali, Università di Milano-Bicocca,
Via R. Cozzi, 53 – 20125, Milano, Italy*

Corresponding authors: *nilius@fhi-berlin.mpg.de
gianfranco.pacchioni@unimib.it

The nano-porous structure of thin SiO₂ films grown on Mo(112) gives rise to an adsorption characteristic that depends on the size of the adsorbates. As revealed by a combined a STM and DFT study, small adatoms such as Pd are able to penetrate the openings in the oxide top-layer and bind strongly to the Mo-SiO₂ interface. Au atoms, on the other hand, are too big and adsorb only at line defects in the oxide surface where the pore size is larger.

The adsorption properties of solid surfaces are dominated by the chemical and physical nature of the topmost atomic plane, while sub-surface layers only weakly contribute to this characteristic. This adsorption behavior is usually unspecific in terms of admitting only selected molecular species for binding or determining well-defined interaction sites on the surface. A much higher degree of surface functionality is common to all biological systems, where foreign species are repelled at the inert surface of a membrane and are allowed to interact only at element-specific pores, e.g. ion channels. A simplified concept of this has been transferred to material science, where a size-selective interaction mechanism was realized for three-dimensional zeolite and silicate structures.¹ The decisive parameter in the process is the pore size of the -Si-Al-O- network, which controls whether a reactant penetrates the opening and propagates to the reaction site or not. Typical pore sizes in zeolites can be adjusted between 1-50 nm, being an ideal diameter for the fabrication of molecular sieves.

No two-dimensional counterpart for a molecular sieve have been produced so far that would be able to control the access of an atomic/molecular species to a reactive subsurface region via nano-pores in the inert top-layer. A selective interaction characteristic would have interesting applications in heterogeneous catalysis, as reaction processes could be steered via the size of the reactants with respect to the openings in the top-layer. A promising candidate for size-specific adsorption is the ultra-thin SiO₂ film on Mo(112), which was recently developed by Schröder et al.^{2,3} and later investigated in detail by experiment and theory.^{4,5,6,7,8} The film is build up by a network of six-membered -Si-O- rings, that is interrupted by eight-membered rings along line defects. The ring opening gives access to the Mo(112) support, which is considerably more reactive than the inert silica layer. According to theoretical predictions,⁹ the possibility to attach adsorbates to the Mo-SiO₂ interface depends on their effective diameter. In this contribution, we demonstrate such size-specific adsorption characteristic of the SiO₂ film by employing scanning tunneling microscopy (STM) and density functional theory (DFT). While Pd atoms are able to penetrate the openings in defect-free oxide patches, Au atoms are too large and only bind at SiO₂ line defects.

The experiments are performed with a costume-built ultra-high vacuum STM operated at 10 K. Electronic properties of the sample are detected with differential conductance

(dI/dV) spectroscopy, providing a measure of the local density of states (LDOS).¹⁰ The SiO₂ film is prepared by depositing 1.2 ML Si in 1x10⁻⁷ mbar O₂ onto an oxygen pre-covered Mo(112) surface and annealing the sample to 1200 K.⁶ Single Au and Pd atoms are deposited onto the cryogenic surface from two separate alumina crucibles. DFT calculations are performed with the generalized gradient approximation as implemented in the VASP code, using the PW91 exchange-correlation functional¹¹ and a plane wave basis set (energy cut-off of 400 eV).¹² The electron-ion interaction is described by the projector augmented wave method.¹³ Various super cells are constructed to model the adsorption properties of SiO₂/Mo(112), in particular a (4x2) cell for Pd (Mo₅₆Si₈O₂₀) and a (5x2) cell for Au adsorption along line defects (Mo₄₀Si₁₀O₂₅). STM images are simulated using the Tersoff-Hamann approach.¹⁰

STM topographic images of the film exhibit a honeycomb structure with protrusions located at each corner of the interlocked hexagons, in agreement with the structure model proposed in [6] (Fig.1A). Each maximum represents the Si atom of a SiO₄ tetrahedron, which is connected to three neighboring Si via bridging O atoms. The fourth O atom located below the Si sits in a bridge position of the $[\bar{1}\bar{1}\bar{1}]$ oriented rows of Mo(112) and anchors the film to the support. The -Si-O- hexagons enclose a hole of 3-4 Å size that opens into a nano-pore at the Mo-SiO₂ interface. The major structural defects of the film are $[\bar{1}\bar{1}0]$ oriented antiphase domain boundaries (APDB), formed by an alternation of eight- (hole size: 5×3 Å²) and four-membered rings (see arrow in Fig.1A).

Adsorption of 0.05 ML of Pd leads to distinct changes in topographic images of the SiO₂ film (Fig.1A). In contrast to earlier experiments, no protruding features are observed that could be associated to single Pd atoms bound to the oxide surface.^{14,15,16} Instead, selected structural elements of the SiO₂ network appear bright, indicating that Pd-induced modifications in the oxide LDOS and not the adatom itself are responsible for the contrast change. This assumption is supported by the pronounced bias dependence of the topographic features associated with Pd (Fig.1C). At negative sample bias (occupied states), the adatom affects only the lower section of a -Si-O- hexagon. At small positive bias, the contrast extends over a larger part of the ring, leading to the emergence of hexangular stars with dark central region. With further bias increase, the bright contrast gradually moves from the edges to the center of the hexagon, where a protrusion becomes

visible above +1.75 V. Pd-induced modifications in the SiO₂ lattice are randomly distributed across the surface and show no preference for either line or point defects. Even for a nominal Pd coverage as high as 0.15 ML, no Pd aggregation or cluster formation is observed. Conductance spectra of the Pd-induced features reveal an increase of the dI/dV signal at 2.3 V with respect to the bare oxide, indicating the presence of a new unoccupied state (Fig.2A). The spatial distribution of the conductance is plotted in the dI/dV map shown in Fig.2B. High Pd-related intensity is observed at 2.3 V, which corresponds to the bias value, where the topographic contrast localizes in the center of a -Si-O- hexagon. The Pd dI/dV signal is swamped by the onset of the silica conduction band at 2.75 V.

DFT calculations of Pd atoms on the silica film rationalize the adsorption characteristics deduced from the experiments. Pd atoms are able to diffuse without barrier through the openings in the six-membered rings and bind to the short Mo-Mo bridge position accessible in the nano-pore (Fig.1B).⁹ The resulting binding energy of 3.3 eV is almost ten times larger than on the silica surface. This strong interaction at the interface is responsible for the ineffective lateral diffusion of Pd atoms, explaining their small preference for oxide defects and the absence of Pd aggregates. Although, the Mo contributes most to the Pd binding, also the electronic states of the oxide ring participate in the interaction. In particular, the 2*p* states of the O atoms in the topmost oxide plane hybridize with the Pd 5*s* orbital, leading to an increase of the unoccupied LDOS between 1.5 - 2.5 eV (Fig.2C). The electronic states of Si-surface and O-interface atoms, on the other hand, remain nearly unaffected upon insertion of the adatom (Fig.2D). This interplay between O and Pd orbitals is responsible for the specific contrast evolution of the -Si-O- rings accommodating a Pd atom, as demonstrated by STM simulations (Fig.1D). As the Pd is located deeply below the oxide surface, the contrast change mainly reflects the adsorbate influence on the silica LDOS, while direct tunneling into Pd orbitals is inefficient. The LDOS contour of the occupied states shows only little change around the Pd adsorption site. However, the adsorbate-induced increase of the unoccupied LDOS leads to the appearance of the typical hexangular stars at positive bias. Structural deformations of the -Si-O- ring, involving a slight relaxation of the O-top atoms towards the embedded Pd, contribute to the electronic alterations.

Only at the resonance position of the *Pd 5s* orbital calculated at +2.0 eV (Fig. 2E), the Pd states directly influence the STM imaging process. The onset of tunneling into this orbital gives rise to the observed dI/dV increase in the Pd conductance spectra. The accessibility of the *Pd 5s*-resonance also leads to the localization of the topographic contrast within the center of the -Si-O- rings, as reproduced in the simulated STM images (Fig.1D).

Exposure of the oxide surface to Au atoms results in a completely different picture (Fig.3A). While no topographic changes are detected on defect-free oxide terraces, protrusions of different size become visible along the APDB. The smallest feature identified with the STM sits in an eight-membered -Si-O- ring and is tentatively assigned to a single Au adatom (Fig.3C, circle). It shows a similar bias-dependent contrast as the Pd species: At small negative bias, two bright spots appear at the long side of the octagon, leaving the nano-pore in the center as a dark hole. With increasing positive bias, the topographic contrast first spreads over larger sections of the ring and then moves towards the ring center, where it forms an elliptical protrusion (Fig.3C). The second smallest aggregate is characterized by an asymmetric shape with respect to the $\text{Mo}[\bar{1}10]$ direction, which indicates occupation of two in-equivalent adsorption sites in the -Si-O-octagon (Fig.3C, square). At higher exposure, larger Au aggregates with spherical shape and negligible bias-dependent contrast develop along the APDB (bottom right of Fig.3A). The Au-related features induce only little change in the dI/dV spectra of the SiO₂ film. The monomer spectrum exhibits a slight increase in the conductance at +1.5 V, similar to the one observed at 2.3 V for Pd. With increasing aggregate size, the dI/dV spectra of the Au species become indistinguishable from the silica background, demonstrating their strong coupling to the support.

Also in the Au case, the experimental findings are well reproduced by DFT. The ‘larger’ Au atoms have to overcome a barrier of 0.9 eV to penetrate a typical six-membered ring.⁹ As this activation energy is higher than the Au binding energy to the SiO₂ of 0.1 eV, the adatoms remain weakly bound to the surface and rapidly diffuse even at low temperature. Only at APDB, exposing eight-membered rings with larger diameter and lower activation energy for penetration (0.15 eV), binding to the Mo-SiO₂ interface becomes possible with 2.67 eV (Fig.3B). The insertion of an Au atom induces again strong modifications in the silica LDOS. In contrast to Pd, these changes are not primarily induced by a direct

hybridization with the Au orbitals, but result from a long-range deformation of the oxide lattice. Not only the atoms of the affected octagon relax outward to allocate more space for the Au, also the adjacent four-membered rings take part in the relaxation process. The structural rearrangement has little effect on the filled states of both O and Si atoms, but increases the unoccupied LDOS of the O atoms in the oxide top layer. This specific LDOS change reflects the widening of the octagon, which reduces the spatial overlap and therefore the hybridization between Si and O orbitals. The four O atoms next to the embedded Au are affected most strongly by the lattice distortion and consequently show up as bright spots in experimental and simulated STM images taken at positive bias (Fig.3D). At voltages above +1.5 V, direct tunneling into Au states becomes important, as revealed by the shift of the topographic contrast towards the ring center and the increase of the dI/dV signal of the Au species. The new channel for tunneling is related to the empty part of the Au 6s orbital, which has split into an occupied and an unoccupied resonance at -0.8 / +0.8 eV due to the interaction with the Mo states.

The nano-pores at APDB are large enough to accommodate a second and third Au atom. The Au dimer adopts a flat configuration with both atoms sitting in a Mo-Mo bridge site. (Fig.3B). The energy gain for attaching the second atom to a pre-adsorbed monomer amounts to 2.48 eV. A third atom binds with 1.77 eV to the bridge position of the Au₂, thus forming a triangular trimer. Based on STM simulations, Au dimers are clearly identified in the experiment (Fig. 3C,D). In images taken at small positive or negative bias, only the upper and central parts of the affected -Si-O- octagon become visible, as these sections are subject to the largest structural deformation. At higher positive bias, the energy levels of Au₂ dominate the tunneling process. Due to hybridization of the two 6s orbitals of the dimer atoms, the lowest accessible state shifts towards E_F with respect to the monomer and the ring center appears with bright contrast already below +0.8 V (Fig.3C). The energy gain when adding atoms to an embedded Au₁ species indicates that APDB are preferential nucleation sites on the SiO₂ film, and the growth of large Au particles decorating the line defects is indeed observed at higher coverage.¹⁷

In conclusion, adsorption of single Pd and Au atoms on a thin SiO₂ film on Mo(112) involves the penetration of the atoms through openings in the silica network and their attachment at the Mo-SiO₂ interface. Due to the different sizes of Au and Pd atoms,

this binding mechanism is active at different positions in the silica film. While Pd is able to pass through the -Si-O- hexagons in defect free oxide patches, the larger Au atoms only enter the eight-membered rings along APDB. The resulting adsorption characteristic resembles a first, primitive form of a molecular sieve, capable of selecting atomic adsorbates via their size.

We thank the COST Action D41 “Inorganic oxides: surfaces and interfaces”. Part of the computing time was provided by the BSC-CNS.

Figure 1

(A) STM image (0.5 V, $13 \times 13 \text{ nm}^2$) of 0.1 ML Pd on SiO_2 on Mo(001). (B) Structure model of the Pd adsorption site (red: O, yellow: Si, light blue: Pd). Bias dependence of the topographic contrast of Pd atoms in (C) experimental ($5 \times 5 \text{ nm}^2$) and (D) simulated STM images ($1.8 \times 1.6 \text{ nm}^2$, 6×4 supercell).

Figure 2

(A) Differential conductance spectra of a Pd atom and bare $\text{SiO}_2 / \text{Mo}(112)$ (set point 2.75 V). (B) dI/dV line scan of the same Pd along the line marked in the inset of (A). (C-E) Calculated LDOS for a Pd atom incorporated into a -Si-O- hexagon. The plots show the contributions of the $2p$ orbital of the O atoms in (C) the top layer and (D) the interface layer (atom positions marked in E). Dashed lines depict the O $2p$ contribution without Pd. (E) Partial LDOS of the Pd $5s,p$ states.

Figure 3

(A) STM image (0.5 V, $13 \times 13 \text{ nm}^2$) of 0.1 ML Au on SiO_2 on Mo(112). (B) Structure model for Au monomer and dimer (red: O, yellow: Si, dark blue: Au). Bias dependence of the topographic contrast for Au aggregates in (C) experimental ($4.5 \times 4.5 \text{ nm}^2$) and (D) simulated STM images ($2.1 \times 1.4 \text{ nm}^2$, 5×4 supercell).

-
- ¹ Bhatia, S. *Zeolite catalysis: principles and applications*, (Boca Raton, 1990, CRC Press); Cheetham, A. K.; Ferey, G.; Loiseau, T. *Angew. Chem. Int. Ed.* **1999**, 38, 3268.
- ² Schroeder, T.; Adelt, M.; Richter, B.; Naschitzki, M.; Bäumer, M.; Freund, H.-J. *Surf. Rev. & Lett.* **2000**, 7, 7.
- ³ Schroeder, T.; Giorgi, J. B.; Bäumer, M.; Freund, H. -J. *Phys. Rev. B* **2002**, 66, 165422.
- ⁴ Kim, Y. D.; Wei, T.; Goodman, D. W., *Langmuir* **2003**, 19, 354.
- ⁵ Ozensoy, E.; Min, B. K.; Santra, A. K.; D. W. Goodman, *J. Phys. Chem. B* **2004**, 108, 4351.
- ⁶ Weissenrieder, J.; Kaya, S.; Lu, J.L.; Gao, H.; Shaikhutdinov, S.; Freund, H.-J.; Sierka, M.; Todorova, T. K.; Sauer, J. *J. Phys. Rev. Lett.* **2005**, 95, 076103.
- ⁷ Giordano, L.; Ricci, D.; Pacchioni, G.; Ugliengo, P. *Surf. Sci.* **2005**, 584, 225.
- ⁸ Lu, J. L.; Kaya, S.; Weissenrieder, J.; Gao, H.; Shaikhutdinov, S.; Freund, H.-J. *Surf. Sci.* **2006**, 600, L153.
- ⁹ Giordano, L.; Del Vitto, A.; Pacchioni, G. *J. Chem. Phys.* **2006**, 124, 034701.
- ¹⁰ Tersoff, J.; Hamann, D. R. *Phys. Rev. Lett.* **1983**, 50, 1998.
- ¹¹ Perdew, J. P.; Chevary, J. A.; Vosko, S. H.; Jackson, K. A.; Pederson, M. R.; Singh, D. J., Fiolhais, C. *Phys. Rev. B* **1992**, 46, 6671.
- ¹² Kresse, G.; Hafner, J. *Phys. Rev. B* **1993**, 47, 558; Kresse, G.; Furthmüller, J. *Phys. Rev. B* **1996**, 54, 11169.
- ¹³ Blöchl, P. E. *Phys. Rev. B* **1994**, 50, 17953.
- ¹⁴ Nilius, N.; Wallis, T. M.; Ho, W. *Phys. Rev. Lett.* **2003**, 90, 046808.
- ¹⁵ Nilius, N.; Rienks, E. D. L.; Rust, H.-P.; Freund, H.-J. *Phys. Rev. Lett.* **2005**, 95, 066101.
- ¹⁶ Sterrer, M.; Risse, T.; Martinez Pozzoni, U.; Giordano, L.; Heyde, M.; Rust, H.-P.; Pacchioni, G.; Freund, H.-J. *Phys. Rev. Lett.* **2007**, 98, 096107.
- ¹⁷ Min, K.; Wallace, W. T.; Santra, A. K.; Goodman, D. W. *J. Chem. Phys. B* **2004**, 108, 16339.

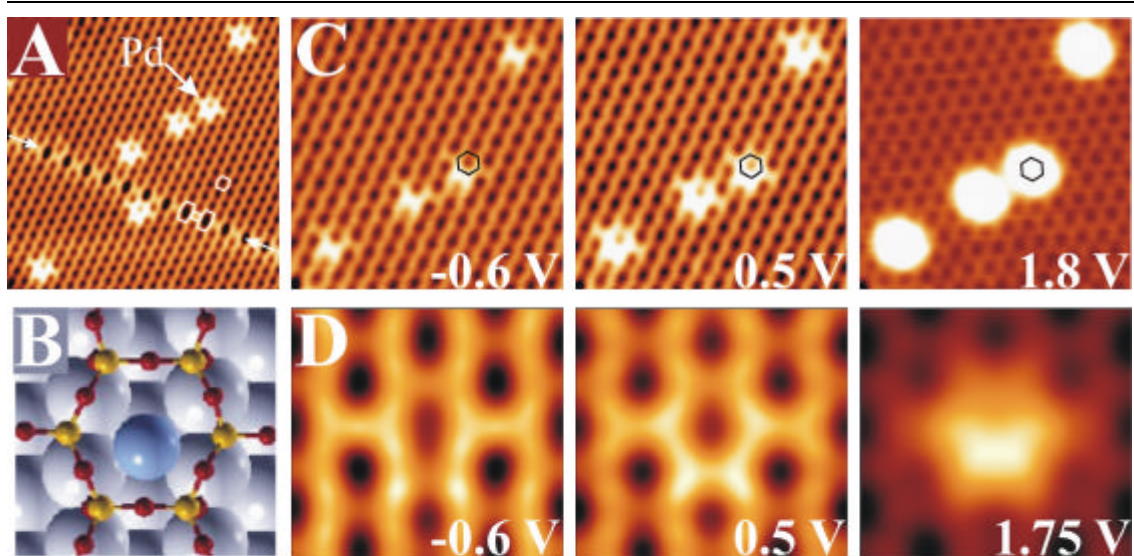


Figure 1

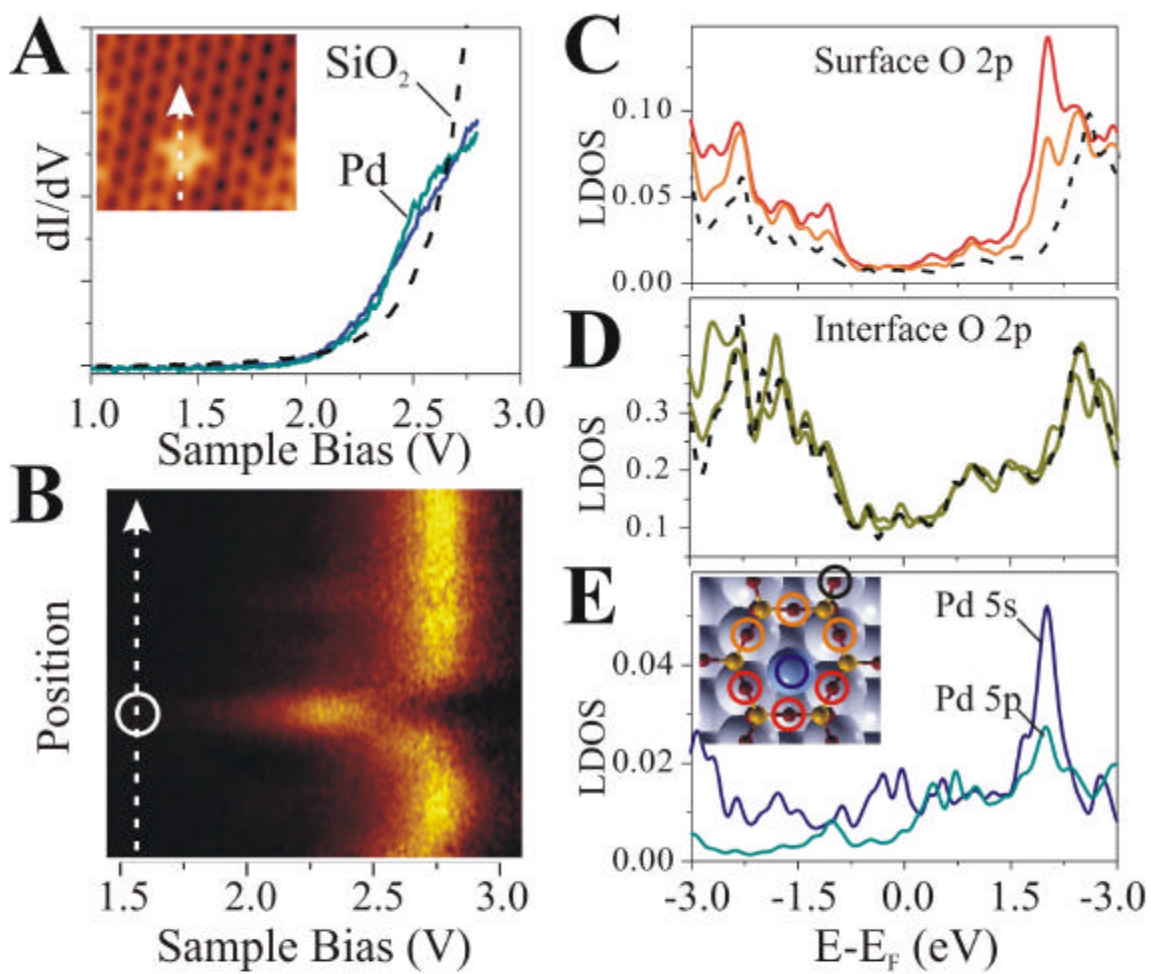


Figure 2

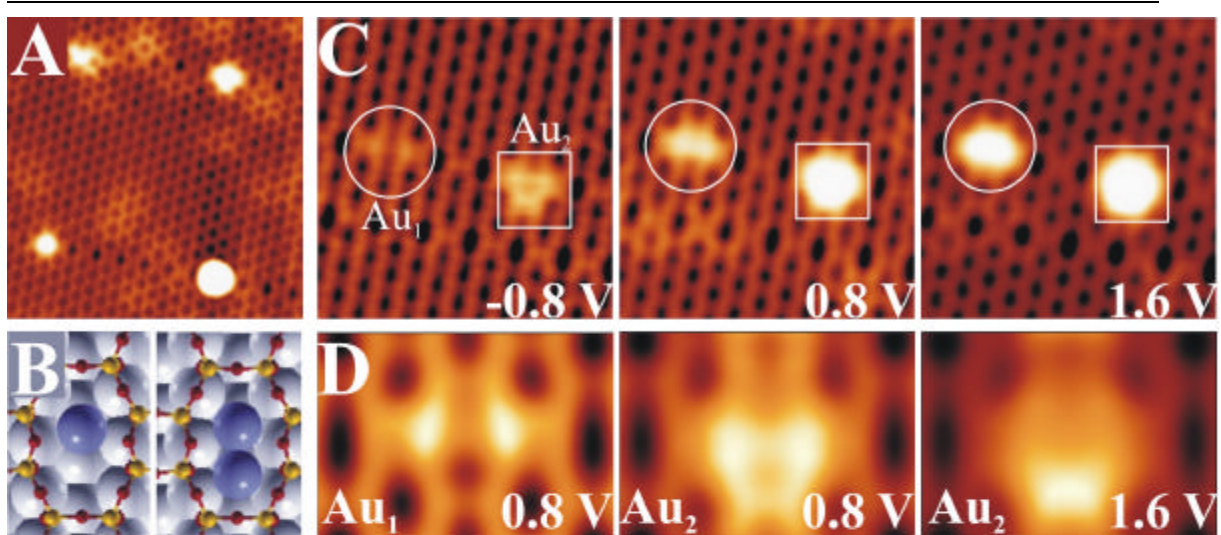


Figure 3